EURO Journal on Computational Optimization 12 (2024) 100089

Contents lists available at ScienceDirect

EURO Journal on Computational Optimization

journal homepage: www.elsevier.com/locate/ejco

Design of experiments for the stochastic unit commitment with economic dispatch models

Nahal Sakhavand [a,*], Jay Rosenberger [a], Victoria C.P. Chen [a], Harsha Gangammanavar [b]

[a] Department of Industrial, Manufacturing and Systems Engineering, University of Texas at Arlington, Arlington, TX-76010, USA
[b] Department of Operations Research and Engineering Management, Southern Methodist University, P.O. Box 750123, Dallas, TX-75275-0123, USA

ARTICLE INFO

Keywords:
Unit commitment
Economic dispatch
Stochastic programming
Design and analysis of computer experiments
Multivariate adaptive regression splines

ABSTRACT

We develop a Design and Analysis of the Computer Experiments (DACE) approach to the stochastic unit commitment problem for power systems with significant renewable integration. For this purpose, we use a two-stage stochastic programming formulation of the stochastic unit commitment-economic dispatch problem. Typically, a sample average approximation of the true problem is solved using a cutting plane method (such as the L-shaped method) or scenario decomposition (such as Progressive Hedging) algorithms. However, when the number of scenarios increases, these solution methods become computationally prohibitive. To address this challenge, we develop a novel DACE approach that exploits the structure of the first-stage unit commitment decision space in a design of experiments, uses features based upon solar generation, and trains a multivariate adaptive regression splines model to approximate the second stage of the stochastic unit commitment-economic dispatch problem. We conduct experiments on two modified IEEE-57 and IEEE-118 test systems and assess the quality of the solutions obtained from both the DACE and the L-shaped methods in a replicated procedure. The results obtained from this approach attest to the significant improvement in the computational performance of the DACE approach over the traditional L-shaped method.

1. Introduction

Renewable energy is a critical resource in power system planning and operations, accounting for more than half of new U.S. power capacity installation [1]. As the fastest-growing energy resource in the United States [2], it offers several benefits for dispatch over conventional resources. The growth is attributed to consistently decreasing installation and operating costs over the past decade. Despite the economic and environmental benefits of renewable resources, their integration on a large scale brings forth several challenges. For instance, the availability of intermittent renewable resources, namely solar and wind, depends on environmental conditions. Consequently, the power generation from these sources exhibits large fluctuations over short time periods. Due to their variability and intermittent nature, predicting generation from solar and wind resources is challenging. Therefore, deterministic optimization frameworks that consider a single-point forecast of uncertainty as input [3] fail to capture the inherent stochasticity of renewable resources. In this regard, Stochastic Programming (SP) approaches have been the subject of interest as they have proved

* Corresponding author.
E-mail addresses: nahal.sakhavand@mavs.uta.edu (N. Sakhavand), jrosenbe@uta.edu (J. Rosenberger), vchen@uta.edu (V.C.P. Chen), harsha@smu.edu (H. Gangammanavar).

https://doi.org/10.1016/j.ejco.2024.100089

Available online 3 May 2024

to provide more realistic solutions while addressing the stochasticity of wind and solar [4]. However, an SP approach exacerbates the computational challenges of optimizing large-scale power system planning and operations problems.

The Unit Commitment (UC) and the Economic Dispatch (ED) models are the main components of planning and operations in power systems. The day-ahead UC problem determines the following day's generation and operating reserve schedules. Formulating UC problems as Mixed-Integer Linear Programming (MILP) models is a common practice. After the commitment decisions are set for the generators and the reserve requirements are met, the dispatch levels of the generators are established as the actual operating interval approaches by solving the ED problem. The dispatch levels are determined while maintaining a balance between supply and demand and adhering to the physical constraints of the power systems components. ED models are typically formulated as linear programming problems [5].

The techniques used to solve Stochastic UC (S-UC) problems have evolved since initially proposed by [6]. Decomposition techniques for S-UC were pioneered by [7] using scenario-based schemes such as the progressive hedging algorithm [8] and later updated by [9] with an augmented Lagrangian. Column generation algorithms, such as the work in [10] have been considered for small-scale test instances with a small set of scenarios. Benders Decomposition (BD) has been applied in a deterministic scheme [11] and for a robust formulation [12]. We refer the interested reader to [13] and [14] for a full review of the S-UC problems. Stochastic ED (S-ED) problems have been frequently modeled with deterministic [15] or probabilistic [16] constraints, and solved using decomposition methods such as Stochastic Decomposition (SD) [17]. Several articles leverage the decomposition-based SP framework to study the combined stochastic unit commitment-economic dispatch (S-UCED) problem [18]. In these works, the UC problem is included in the first stage to determine the commitment decisions. In the second stage, the ED problem is solved in response to a selected commitment decision and a realization of the uncertainty. More recent research in [19] presents a stochastic and simulation-based framework that uses the L-shaped method [20] to solve the S-UCED problem.

The SP models for S-UCED aim to identify commitment decisions that are well-hedged against uncertainty, primarily due to demand and renewable generation. The S-UCED models use continuous random variables to model demand and renewable generation. Therefore, the resulting expectation-valued objective function involves high-dimensional integration. For computational tractability, a suitable representation of the underlying random variables is generated using sampling-based methods (e.g., Monte Carlo sampling) *a priori* to optimization. A finite and fixed sample of scenarios represents the continuous random variables. The resulting optimization problem is the Sample Average Approximation (SAA) [21]. Once the SAA problem is generated, decomposition (stage or scenario) methods can be employed to solve the approximate problem. This approach has been used in several S-UC [22] and S-ED [23] problems.

Traditional cutting-plane algorithms, such as the L-shaped method, generate affine lower bounding functions or cuts to approximate the expected recourse function value. These cuts are added to the master problem as constraints. As the algorithm progresses, the size of the master problem grows linearly, and therefore, the computational difficulty grows significantly as the number of iterations increases. In contrast to the stage-decomposition approach of the L-shaped method, the progressive algorithm involves solving individual scenario problems, a primal aggregation, and a dual multiplier update step. However, the performance of progressive hedging, particularly on S-UC problems, is known to be sensitive to the parameters used in the dual multiplier update step [24]. These decomposition methods apply only when the underlying support is finite or when the SAA problem is being solved. Given the notoriously challenging NP-hard nature of stochastic MILP problems, solving realistically large-scale S-UCED problems remains challenging.

An alternative approach to ease the computational effort is to apply design and analysis of computer experiments (DACE). The DACE approach was first proposed by [25] and later suggested by [26] for SP models to accelerate the convergence over the traditional methods. The use of the DACE approach has shown to be appealing in solving certain two-stage SP models, such as the work studied in [27]. This approach exploits a metamodel as a surrogate to approximate the expectation-valued objective function of the SP model given the design parameters. An optimally equivalent value function using MARS is presented in [28]. Several other papers have also benefited from a DACE-based optimization approach to solve their complex models [e.g., 29,30].

To construct the metamodel, one must implement two primary steps: (1) use an experimental design to select a set of sample points that cover the parameters' feasible region known as the design space, and (2) fit a statistical model to the output of the observed sample points [31]. The common Design of Experiments (DoE) techniques that can be used to fill the design space include Latin hypercubes, orthogonal arrays, and number-theoretic methods. The Latin hypercube design was first proposed in [32]. Later, [33] extended the design for the case of a continuous range of each variable using a uniform distribution over each interval. For a full review on selecting an appropriate experimental design and statistical model for constructing a metamodel, we refer the interested reader to [34].

In an optimization model, such as SP models, constraints form a feasible region that is not a hypercube, unlike the aforementioned DoE approaches. Consequently, developing a DoE approach to represent the design space in an SP model is not straightforward and requires exploiting properties of the first-stage decision space. The authors are aware of only one other research paper that develops a DoE approach over a feasible region that is more complicated than a hypercube. Specifically, [35] develops a mixed design that handles the specific constraints in the commercial airline fleet assignment problem.

As for the statistical modeling step, common statistical methods include but are not limited to regression trees and Multivariate Adaptive Regression Splines (MARS). MARS as a non-parametric algorithm was first proposed by [36], which creates a piecewise linear model to discover the relationships between a response value and the predictors that are additive or involve predictor interaction effects. To our knowledge, our suggested approach is the first DACE-based optimization that considers the actual structure of the UC decision space to create a DoE algorithm. Moreover, our DACE-based optimization provides a flexible approximation of the UC model, which can be globally optimized [30].

It is worthwhile to note that unlike the decomposition methods (L-shaped and progressive hedging), the DACE approach does not rely on the finiteness of the underlying stochastic process. In this regard, DACE approaches may aim to solve problems that do not necessarily approximate the uncertainty with a finite discrete support set.

Compared with existing literature, the main contributions made in this research are as follows:

- We present a heuristic DACE-based optimization approach that uses a metamodel to approximate the expected recourse function in the two-stage S-UCED model. The first stage of the formulation corresponds to the unit commitment. We determine these decisions before observing a realization of the uncertainty in renewable generation. Subsequently, we model the dispatch procedure in the second stage. The second stage responds to a fixed commitment decision and a realization of the uncertainty in renewable generation. To the best of our knowledge, our work provides the first application of the DACE approach to the S-UCED problem. Moreover, we customize our approach to take advantage of the special structure in the first stage to generate the DoE for the unit commitment problem. We utilize these features to predict the second-stage recourse function value. Although this approach is developed for the S-UCED problem, it is likely applicable to other systems with a finite set of machines or devices with minimum and maximum on and off periods.
- We fit our statistical model for the expected recourse function using MARS. This model controls the number of subproblems to solve in the second stage, which is impossible to track in traditional cutting-plane algorithms such as the L-shaped method. In addition, our model develops an understanding of the relationship between the recourse function and the input space. In particular, the relationship between commitment decisions favors developing special features on how long the generators operate and their status in certain periods based upon changes in renewable generation. This can also assist in identifying the generators that have the most impact on the potential operating costs.
- We compare our results with the well-recognized L-shaped method. Using the DACE approach reveals a significant reduction in the computing time over the traditional L-shaped method on two standard test instances with a large set of scenarios. This allows the system operators to make planning and operational decisions within the tight time frame in the electricity market.

The rest of the paper is organized as follows. In Section 2, we present the UC model. Section 3 provides a general framework of the S-UCED model, a comprehensive description of the DACE-based approach used to solve the problem, followed by presenting the numerical results in Section 4. Finally, we conclude the paper in Section 5 with a brief discussion on future trends.

2. Problem formulation

This section presents the first stage problem, i.e., the UC problem formulation. For our purpose, we consider a power system with buses (nodes) denoted by $\mathcal{B}$ and transmission lines denoted by w. We denote the subset of nodes that connect to loads by $\mathcal{D}$. Finally, we denote by $\mathcal{G}$ and $\mathcal{R}$ the sets of conventional and renewable generators, respectively. We use $\mathcal{T}$ to denote the set of decision epochs within the problem horizon. The presented UC formulation is based on [37]. This formulation uses a state transition concept that emphasizes the transition of the generator status between two consecutive time periods, leading to better performance in longer planning horizons with variable demand patterns compared with those in the literature. Our DACE approach exploits this formulation to obtain reliable information on the potential operating costs and the detailed status of the generators in extensive horizons. For a generator $g \in \mathcal{G}$, we define the state decision variable $x_{g,t}$. It takes a value of one if the generator remains operational in time period $t \in \mathcal{T}$; otherwise, it takes a value of zero. Binary variables $s_{g,t}$ and $z_{g,t}$ denote the generator start-up and shut-down variables, respectively. These variables take a value of one if the generator is switched on (or off) in time period $t \in \mathcal{T}$, and zero otherwise. Using these variables, it is possible to represent the transition of the generator state in one period to the next on a network. With this perspective, the state transition is captured by the following flow balance equation:

$$s_{g,t-1} + x_{g,t-1} = z_{g,t} + x_{g,t} \qquad \forall g \in \mathcal{G},\ t \in \mathcal{T}. \tag{1}$$

The common constraints incorporated in the UC problem capture the restrictions imposed by the underlying physics. The minimum downtime/uptime constraints enforce the requirement for a unit to stay on/off for a minimum amount of time. These are given by

$$\sum_{i=t-UT_g+1}^{t-1} s_{g,i} \le x_{g,t} \qquad \forall g \in \mathcal{G},\ t \in \mathcal{T}, \tag{2a}$$

$$\sum_{i=t-DT_g}^{t} s_{g,i} \le 1 - x_{g,t-DT_g} \qquad \forall g \in \mathcal{G},\ t \in \mathcal{T}. \tag{2b}$$

Here, UT_g and DT_g are the minimum uptime and downtime limits, respectively, that are characteristic of a generator g. Constraint (2a) ensures that a generator that is operational in time period $t-1$ and continues to be operational in time period t (i.e., $x_{g,t} = 1$) could have been turned on at most once in the previous $UT_g - 1$ time periods. Similarly, constraint (2b) suggests that if a generator remains operational, it cannot be switched on again in the current time period t or the next DT_g time periods. In our formulation, the generator cannot be turned on and off simultaneously; therefore, $UT_g \ge 1$ and $DT_g \ge 1$.

We define two variables to capture the generation amount in the UC problem. The use of two separate generation variables allows us to capture all necessary information to formulate the system reserve requirement. Specifically, the first variable, denoted by $G'_{g,t}$,

captures the amount of generation beyond the minimum capacity of an operational generator (denoted by $\underline{C}_g$). Since we consider a stochastic setting, we may revise the generation amount determined in the UC stage during dispatch. Furthermore, the committed generators can also act as spinning operating reserves to cover the discrepancy between the forecast and actual renewable generation. The second variable captures the maximum generation that a generator can produce to cover any shortfall in renewable generation. We denote this variable as $\overline{G}_{g,t}$. Typically, the power system operators require a certain minimum amount of spinning reserves to be committed to the UC problem. We denote the required reserve amounts by ρ_t. These maximum generation decision variables must satisfy

$$\sum_{g\in\mathcal{G}} \overline{G}_{g,t} \geq \left(\sum_{i\in\mathcal{D}} D_{i,t} - \sum_{i\in\mathcal{R}} \check{G}_{i,t} \right) + \rho_t \qquad \forall t \in \mathcal{T} \tag{3}$$

where $\check{G}_{i,t}$ is the forecast of renewable generation from $i \in \mathcal{R}$, and $D_{i,t}$ is the demand at node $i \in \mathcal{D}$. The term in parentheses on the right-hand side of the inequality (3) is often referred to as the net demand that represents the amount the generation expected to be met by the conventional generation resources.

The maximum generation $\overline{G}_{g,t}$ and the generation amount $G'_{g,t}$ are variables related to the on and off status of the generator through the following constraints:

$$\overline{G}_{g,t} \geq G'_{g,t} + \underline{C}_g(s_{g,t} + x_{g,t}) \qquad \forall g \in \mathcal{G},\ t \in \mathcal{T}, \tag{4a}$$

$$\overline{G}_{g,t} \leq \overline{C}_g(s_{g,t} + x_{g,t}) + (\underline{S}_g - \overline{C}_g) z_{g,t+1} \qquad \forall g \in \mathcal{G},\ t \in \mathcal{T}. \tag{4b}$$

In the above, $\overline{C}_g$ is the maximum generation capacity when g is operational. Additionally, $\overline{S}_g$ and $\underline{S}_g$, respectively, denote the maximum and minimum capacity that a generator must meet upon startup and before it is shutdown. The following demand constraints ensure the expected net demand is met by the committed conventional generators and is presented as follows:

$$\sum_{g\in\mathcal{G}} (G'_{g,t} + \underline{C}_g(s_{g,t} + x_{g,t})) \geq \left(\sum_{i\in\mathcal{D}} D_{i,t} - \sum_{i\in\mathcal{R}} \check{G}_{i,t} \right) \forall t \in \mathcal{T}. \tag{5}$$

Finally, the ramping constraints relate the generation amounts from one time period to the next for all the committed conventional generators. These constraints are given by:

$$\overline{G}_{g,t} - G'_{g,t-1} \leq \overline{S}_g s_{g,t} + (\overline{R}_g + \underline{C}_g) x_{g,t} \qquad \forall g \in \mathcal{G},\ t \in \mathcal{T}, \tag{6a}$$

$$G'_{g,t-1} - G'_{g,t} \leq (\underline{S}_g - \underline{C}_g) z_{g,t} + \underline{R}_g x_{g,t} \qquad \forall g \in \mathcal{G},\ t \in \mathcal{T}, \tag{6b}$$

where $\overline{R}_g$ and $\underline{R}_g$ are the ramp-up and ramp-down limits. Constraint (6a) ensures that the increase in the generation output of the remain-on generator is limited by $\overline{R}_g$. On the other hand, the generation of a generator that is switched on is bounded by $\overline{S}_g$. Notice the use of the maximum generation variable $\overline{G}_{g,t}$ in formulating the ramp-up constraints. This is done to ensure that there is sufficient ramping capability even when reserves are needed. The constraint (6b) ensures that the decrease in the generation of a remain-on generator is limited by the ramp-down limit $\underline{R}_g$. The constraint also ensures that a generator that is switched off in time period t does not generate more than $\underline{S}_g$ in the previous time period.

Once the commitment decisions are made, these decisions are passed to the second stage, where an ED problem is solved. Notice that we only use the commitment decisions $\mathbf{u} = (x_{g,t}, s_{g,t}, z_{g,t})_{\forall g\in\mathcal{G}, t\in\mathcal{T}}$ as the linking variables, and generation decisions can be revised in response to the observed scenarios of the renewable generation. We refer the reader to Appendix A for the full table of the parameters and decision variables, and Appendix B and Appendix C for the formulation of the ED as well as the detailed combined S-UCED problem.

3. The DACE approach

For the purpose of illustrating our DACE solution, we use the following general two-stage SP form with a mixed-binary first stage and a continuous recourse.

$$\begin{aligned} \min\ & f(\mathbf{u},\mathbf{v}) := c(\mathbf{u},\mathbf{v}) + \mathbb{E}\{Q(\mathbf{u},\tilde{\xi})\} \\ \text{s.t } & \mathbf{u} \in \mathcal{U} := \{\mathbf{u}' \text{ satisfy (1) and (2)}\} \\ & (\mathbf{u},\mathbf{v}) \in \mathcal{V} := \{(\mathbf{u}',\mathbf{v}') \text{ satisfy (3)} - \text{(6)}\}, \end{aligned} \tag{7a}$$

where the uncertain demand and renewable generation is represented by $\tilde{\xi}$, and the recourse function is the optimal value of the following problem:

$$\begin{aligned} Q(\mathbf{u},\xi) = \min\ & d(\mathbf{y},\xi) \\ \text{s.t } & W\mathbf{y} = r(\xi) - T\mathbf{u},\ \mathbf{y} \in \mathbb{R}^{n_2}_+. \end{aligned} \tag{7b}$$

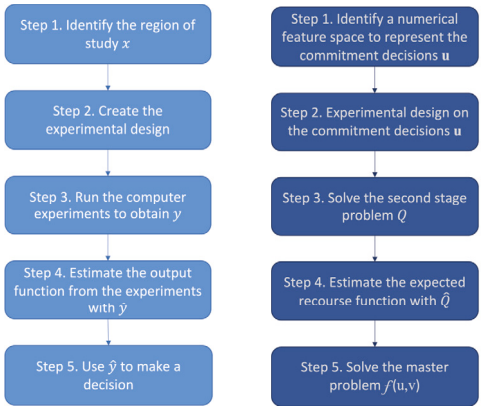

(a) DACE approach procedure (b) DACE approach for S-UCED

Fig. 1. The detailed steps of the DACE approach.

In the above general form, we distinguish between the binary commitment decision variables, $\mathbf{u} = (x_{g,t}, s_{g,t}, z_{g,t})_{\forall g \in \mathcal{G}, t \in \mathcal{T}}$, and first-stage continuous decision variables captured by $\mathbf{v} = (G'_{g,t}, \bar{G}_{g,t})_{\forall g \in \mathcal{G}, t \in \mathcal{T}}$. The second-stage continuous decision variables, denoted by $\mathbf{y}$, are determined adaptively after the realization of the random vector $\tilde{\xi}$ denoted by ξ is revealed. We assume that the $\tilde{\xi}$ is defined over the probability space $(\Xi, \mathcal{F}, P)$, where Ξ is the sample space and corresponds to the set of random variable outcomes, $\mathcal{F}$ is the sigma-algebra, and P is the probability measure function. Notice that the two-stage SP form of S-UCED satisfies fixed and relatively complete recourse. The former implies that the recourse matrix W is deterministic. The latter implies that the second-stage program is feasible for any first-stage decision $(\mathbf{u}, \mathbf{v}) \in \mathcal{V}$ and observation $\xi \in \Xi$. The feasibility of the ED problem is attributed to the ability to shed excess generation and curtail load (see (B.4) and the subsequent discussion). Relatively complete recourse is desirable in DACE as it allows us to utilize most of the design points generated by the experimental design, as we will see later in the section. Design of experiments is typically conducted using variables in which every permutation of the variables has a numeric response. Consequently, when using DACE for two-stage stochastic programming, we wish to have a design of experiments over a large subset of the first-stage variables such that both stages are feasible and that the recourse function yields a numeric response value. Relatively complete recourse will yield a numeric response value for each design point that is feasible in the first stage. In S-UCED, notice that only the right-hand side of the second-stage constraints has random elements (random demand and renewable generation). However, determining a design of experiments in which every design point is feasible in the first stage may be challenging. In this research, we construct a design in which every point satisfies (1) and (2) but may be infeasible for (3) – (6).

A high-level DACE framework is introduced in [26] that describes a rigorous numerical solution method for high-dimensional SP models. In general, computer experiments involve adapting the original physical experiment with the same concepts that consist of defining the study region, identifying the appropriate experimental design method, collecting the data, conducting the data analysis and ultimately drawing conclusions based on the analysis. We refer the interested reader to [38] for more details on design and analysis of experiments. However, the applicability of this general framework to the S-UCED problem is not straightforward, so in this research, we exploit the special structure of the S-UCED problem to develop a customized DACE-based approach. Fig. 1a illustrates the high-level framework, and Fig. 1b summarizes the adapted version of this approach applied to the model in (7). One challenge of applying the DACE approach to the S-UCED problem is that the input (x) and output (y) of the algorithm in the DACE approach are generally assumed to be numerical. In our case, the region of study in the first stage (7a) is a binary space. To tackle the intractability of modeling over a high-dimensional binary space, we introduce a numerical feature space to represent the commitment decisions. In addition, the numerical feature space allows us to use the MARS statistical model as an approximation. Further, DoE ideally desires an orthogonal space, which includes no multicollinearity in the feature space to enable causal modeling. Since the constraints in (7) directly impose collinear structure, DoE is conducted over a more controllable space from which the commitment decisions are derived and then used as input to the second stage optimization problem to obtain feasible recourse values for Step 3 in Fig. 1b. These recourse values are then used to obtain the predicted value of $\hat{y}$. The resulting MARS statistical model that estimates the expected recourse function can then be globally optimized.

3.1. Defining the feature space

In this section, we describe Step 1 of the flowchart in Fig. 1b. For the DACE process, the feature space must be appropriately specified to enable a good estimate of the recourse function in Step 4. In our case, the most straightforward feature space consists of (x_{gt}, s_{gt}, z_{gt}) for every unit g at time period t that satisfies the first stage constraints of (7a). However, there are three concerns with employing the commitment decisions directly as the DACE feature space. First, the original binary space is high-dimensional, involving $3|\mathcal{G}||\mathcal{T}|$ variables. Second, these features are binary, and while it is possible to conduct DoE for a binary feature space, this

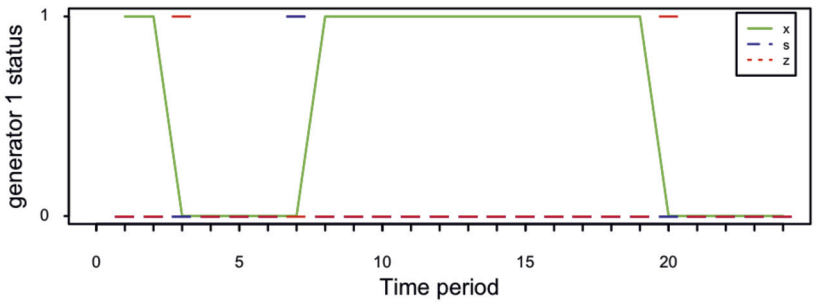

Fig. 2. Commitment status for generator 1 in a 24-hour period.

will not enable a good approximation in Step 4 in the DACE approach. Finally, as previously mentioned, the commitment decisions are collinear variables. This is specifically noticeable in the state transition constraints (1) that link these variables and the minimum downtime and uptime constraints (2). The inevitable multicollinearity of such a large number of predictors renders a good DoE impossible and would result in an unstable approximation model in Step 4 [39,40]. To overcome these challenges, we partition the day into time intervals denoted by $\mathcal{I}$. For each interval $i \in \mathcal{I}$, we use $\mathcal{T}_i$ to denote its time periods. For any time interval i, we define a numerical input space by introducing nonnegative integer features w_{gi} that capture the number of time periods at which unit g remains on within that interval. The new *commitment linking* feature space has $|\mathcal{G}||\mathcal{I}|$ variables. These variables are mapped to the first-stage variable space through the following constraint in the optimization model.

$$w_{gi} = \sum_{t \in \mathcal{T}_i} x_{g,t} \qquad \forall g \in \mathcal{G} \qquad \forall i \in \mathcal{I}. \tag{8}$$

Moreover, because power system problems, particularly solar generation, typically have daily cyclical characteristics, the partitioning of the day into time periods can be done with consideration of a daily cycle. We present such a partitioning in Section 4.

3.2. Generating the experimental design

This section details Step 2 of the flowchart in Fig. 1b. In general, the DoE procedure, which selects a set of sample points, requires specification of the range on the feature space over which the DoE is constructed as input to the optimization model. Given our feature space defined by the commitment linking variables w_{gi}, the challenge here is identifying a reasonable range as is normally determined in a traditional DoE procedure. Specifically, a DoE for the first-stage S-UCED problem that selects sample values of w_{gi} without regard to the UC decision constraints, namely (1)–(2), will likely lead to many points that violate these constraints. Consequently, instead of directly constructing DoE over the w_{gi} variables, the available generator data can be utilized to identify the consecutive periods of uptime and downtime. DoE is then used to sample hypothetical sequences of uptime and downtime for each generator, and the commitment linking variables w_{gi} can then be calculated based on these sequences. Let the minimum length of consecutive periods required for generator g to remain on and off be MinUT_g and MinDT_g, respectively. This definition is synonymous with minimum uptime and downtime discussed in the UC problem. Subsequently, let the maximum number of consecutive time periods that generator g requires to remain on and off be MaxUT_g and MaxDT_g, respectively, over the course of the 24-hour horizon. In our experiments, we have set $\text{MaxUT}_g = \mathcal{T}$, $\forall g \in \mathcal{G}$, and $\text{MaxDT}_g = \mathcal{T}$, $\forall g \in \mathcal{G}$.

For each generator g, we use MinUT_g and MinDT_g data to identify the maximum number of changes in the commitment status of each generator from remaining on to remaining off and vice-versa. For instance, if MinUT_g is two hours and MinDT_g is one hour, then there can be at most fifteen status changes in a 24-hour horizon, with at most seven switch-on and eight switch-off changes. We denote by Ω_g to be the maximum number of switch on or switch off status changes. Furthermore, we introduce $\overline{\omega}_g$ and $\underline{\omega}_g$ to denote random variables in the experimental design process that correspond to the uptime and downtime, respectively. The random variable $\overline{\omega}_g$ is defined over the support $[\text{MinUT}_g, \text{MaxUT}_g]$. Similarly, $\underline{\omega}_g$ is defined over the support $[\text{MinDT}_g, \text{MaxDT}_g]$. We can generate a sequence of $2 \times \Omega_g$ outcomes using these random variables. If the generator remains on during a current time period t, and is off in the next time period $t+1$, the unit must have been switched off at the beginning of period $t+1$; i.e., $z_{g,t+1} = 1$. We can obtain the switching on of the unit g denoted by $s_{g,t}$ in a similar manner. Therefore, the corresponding values of $z_{g,t}$ and $s_{g,t}$ can be derived from the value of $x_{g,t}$ for the unit g at a particular time t. We leverage this fact in constructing the LHS design. Notice that an observation is a realization of the duration of uptime and downtime sequences for a generator. Given an observation, we can construct the features (UC decision vector) of $(x_{g,t}, s_{g,t}, z_{g,t})$ for the entire 24-hour horizon. We capture this construction using a mapping ϕ which we illustrate through an example. Consider the following observation $\mathcal{O}_g = (2, 5, 12, 5, 0, 0)$. The feature values are shown in Fig. 2. Notice since $\overline{\omega}_{g,1} = 2$, the generator remains on for the first two time periods, and it's switched off in the third time period; therefore, $z_{g,3} = 1$. Since $\underline{\omega}_{g,1} = 5$, the generator remains off until $t = 7$. It is then switched on, resulting in $s_{g,7} = 1$.

We simulate Ω_g outcomes of $\underline{\omega}_g$ and $\overline{\omega}_g$ and arrange them in an alternating order. We refer to the resulting sequence as an *observation*. If $\{\underline{\omega}_{g,1}, \underline{\omega}_{g,2}, \ldots, \underline{\omega}_{g,\Omega_g}\}$ are the simulated outcomes of $\underline{\omega}_g$ and $\{\overline{\omega}_{g,1}, \overline{\omega}_{g,2}, \ldots, \overline{\omega}_{g,\Omega_g}\}$ are the outcomes of $\overline{\omega}_g$, then an observation will have the following form:

$$\mathcal{O}_g = (\underline{\omega}_{g,1}, \overline{\omega}_{g,1}, \underline{\omega}_{g,2}, \overline{\omega}_{g,2}, \ldots, \underline{\omega}_{g,\Omega_g}, \overline{\omega}_{g,\Omega_g}).$$

We use Latin Hypercube Sampling (LHS) design [33] to generate a set of N observations. An experimental design is a matrix, with columns representing the different dimensions of the design space and the rows representing the realized sequences. Here, the dimension of the design space is $2\sum_g \Omega_g$ to accommodate both the observations for all the generators. For our LHS design, we generated N observations (N rows in the design matrix). The experimental design is standardized to a range of values between 0 and 1. For a column representing uptime for a specific generator, the value is scaled to its support, i.e., $[\text{MinUT}_g, \text{MaxUT}_g]$. Similarly, if a column represents downtime, the value is scaled to its support $[\text{MinDT}_g, \text{MaxDT}_g]$. Since we consider one-hour time steps, we round the resulting realization to the nearest integer. We summarize these steps in Algorithm 1.

Algorithm 1: Experimental design with LHS.

Input: Generator data $\text{MinUT}_g, \text{MaxUT}_g, \text{MinDT}_g, \text{MaxDT}_g$, Ω_g for $\{g \in \mathcal{G}\}$; the number of observations, N.
for $\{g \in \mathcal{G}\}$ **do**
  Step 1. Construct a LHS design with dimension $2\Omega_g$; with interval $[\text{MinUT}_g, \text{MaxUT}_g]$, $[\text{MinDT}_g, \text{MaxDT}_g]$ for random variables $\overline{\omega}_g$ and $\underline{\omega}_g$, respectively; N discritizations (levels).
  for $n = 1, \ldots, N$ **do**
    Step 2. Construct observations $\mathcal{O}_g^n$.
    Step 3. Compute $\phi(\mathcal{O}_g^n) = (x_{gt}^n, s_{gt}^n, z_{gt}^n)$.
Output: Features (UC decisions) for all generators and time periods.

The final sampled set of DoE points must lie within the feasible region of the first stage (7a). Specifically, while a DoE point, say $\bar{\mathbf{u}}$, generated in Step 1 of Algorithm 1 lies in $\mathcal{U}$, we need to verify that the set $\mathcal{V} \neq \emptyset$ with $\mathbf{u} = \bar{\mathbf{u}}$. To ensure that DoE points satisfy the above requirement, we solve the following mean value problem, which provides optimistic solutions for (7).

$$\min_{(\mathbf{u},\mathbf{v})\in\mathcal{V}} f(\mathbf{u},\mathbf{v}) := c(\mathbf{u},\mathbf{v}) + Q(\mathbf{u},\bar{\xi}), \tag{9}$$

where $\mathbb{E}\{\tilde{\xi}\} = \bar{\xi}$. The optimal objective function value of the mean value problem provides a lower bound for the expected recourse value. This follows from the fact that Q is a convex function in ξ, allowing us to invoke Jensen's inequality [21]. Hence, we use the optimal commitment solutions of (9) as a baseline for our DoE procedure to identify the conventional generators that always remain on (i.e., $x_{g,t} = 1$ for $t \in \mathcal{T}$). This approach retains feasibility of commitment decision $\mathbf{u}$ with respect to (1) and (2) that are specific to individual generators. Therefore, these solutions are used to initialize the DoE approach. Note that solutions that are first-stage feasible and yield non-empty second-stage feasible region can serve as DoE points. Nonetheless, while this approach may encourage first-stage feasibility of constraints in (3) – (6), it does not guarantee that every design point is feasible. Approaches alternative to the mean value solution are worth a complete discussion and are recommended for future research.

3.3. Approximating the recourse function

This section describes Steps 3 and 4 of the DACE flowchart in Fig. 1b. Once we simulate the design points and map them to the commitment decision space of $(\mathbf{x}, \mathbf{s}, \mathbf{z})$ in Step 2, we solve the second stage problem (7b) to obtain the corresponding recourse values Q for each observation n in Step 3. Similarly, for each observation n, $\mathbf{w}^n$ is calculated using (8). Consequently, the data defined by the tuples $\{\mathbf{w}^n, Q(\mathbf{x}^n, \mathbf{s}^n, \mathbf{z}^n)\}_{n=1}^N$ are used to estimate an approximate recourse function $\hat{Q}(\mathbf{w})$ in the $\mathbf{w}$ domain. The MARS approach provides an accurate approximation of the relationships between the predictor variables for complex optimization models [29,41]. To approximate the second stage problem in Step 4, we use the MARS approximation to fit to the recourse response values, Q, with the aforementioned data. Because MARS is non-interpolating, we need not be concerned with multiple w-vectors with different associated second-stage objective values.

The MARS statistical model is a weighted sum of basis functions We can write the MARS model for the expected recourse function accordingly:

$$\hat{Q}(\mathbf{w}) = \sum_{j=0}^{J} a_j B_j(\mathbf{w}), \tag{10}$$

where $B_j(\mathbf{w})$ and a_j are the j-th basis function and the coefficient, respectively. The basis functions can be the form of a constant, a univariate hinge function, or a product of two or more univariate functions. In our case, we can write the j-th basis function as follows:

$$B_j(\mathbf{w}) = \prod_{m=1}^{M_j} b_{m,j}(\mathbf{w}), \tag{11}$$

where M_j is the number of univariate hinge functions $b_{m,j}$. The univariate hinge functions have a cutpoint value (or knot) k at which the $\hat{Q}$ function bends and modeled as

$$b_{m,j}(\mathbf{w}) = \max\{0, \pm(w_{gi(m,j)} - k_{m,j})\}. \tag{12}$$

To train the model in the MARS procedure, a single point across the range of the input values, $\mathbf{w}$, is selected where two different relationships between the commitment values and the recourse function yield the smallest error. The set of candidate basis functions is chosen iteratively, basically a collection of the predictor variables w_{gi} and the knots. Truncated linear basis functions are added until the MARS model that best fits the data is achieved using a lack-of-fit criterion and also a specified maximum number of basis functions. Subsets of basis functions are explored until we reach a balance of bias and variance in the model. For more information on MARS, see [27] and [36].

3.4. Optimization of the approximated S-UCED model

Consider the S-UCED problem in (7) again. The derived predicted model in Step 3 is an approximation of the expected recourse function, i.e., $\hat{Q}(\mathbf{w}) \approx \mathbb{E}\{Q(\mathbf{u}, \tilde{\xi})\}$.

The last step in the DACE approach is to optimize the resulting model, which consists of the first stage cost function as well as the MARS approximation $\hat{Q}(\mathbf{w})$ for the second stage.

$$\begin{aligned} &\min \ f(\mathbf{u}, \mathbf{v}) := c(\mathbf{u}, \mathbf{v}) + \hat{Q}(\mathbf{w}) \\ &\text{s.t } \mathbf{u} \in \mathcal{U}, (\mathbf{u}, \mathbf{v}) \in \mathcal{V} \\ &\quad w_{gi} = \sum_{t \in \mathcal{T}_i} x_{g,h} \qquad \forall g \in \mathcal{G} \qquad \forall i \in \mathcal{I}. \end{aligned} \tag{13}$$

It can be shown that if $\hat{Q}(\mathbf{w})$ is constructed using a non-smooth and Two-way Interaction Truncated Linear (TITL) form of the MARS function, (13) can be formulated as a Mixed-Integer Quadratic Programming (MIQP) model and therefore, globally optimized. For each univariate basis functions, b, the MIQP uses a binary variable indicating whether the w term is above or below the knot k and a continuous variable to represent the value of the basis function. In general, the complexity of both the MARS model and the corresponding MIQP is based upon the complexity of the recourse function Q. For a full description of using MIQP to formulate and solve $\hat{Q}(\mathbf{w})$, we refer the interested reader to [30].

3.5. Solution quality assessment

Let us revisit the S-UCED problem in (7). For computational tractability, the expectation in the objective function is often replaced by a sample average computed using a set of random scenarios $\Xi_{n'} \subseteq \Xi$ of demand and renewable generation. Here, n' is the size of the random sample. The resulting problem is the SAA of the S-UCED and is written as

$$f_{n'}(\mathbf{u}, \mathbf{v}) = \min_{(\mathbf{u},\mathbf{v}) \in \mathcal{V}} \left\{ c(\mathbf{u}, \mathbf{v}) + \frac{1}{n'} \sum_{i=1}^{n'} Q(\mathbf{u}, \xi_i) \right\}. \tag{14}$$

We denote the optimal value of the true two-stage SP model and the SAA by a^* and $a^*_{n'}$, respectively.

Since the sample is generated randomly, the resulting solutions and values are stochastic. Therefore, assessing the quality of the solutions obtained from the optimization process is necessary. A multiple replication-based procedures was introduced in [42] for assessing the quality of solutions obtained from a sampling-based approach. Later, the term SAA was proposed by [43]. As presented in [42], in an M-replicated procedure, we generate M samples of independent identically distributed (iid) observations $\{\xi^m_1, \xi^m_2, ..., \xi^m_{n'}\}$, each of size n'. Using these observations, we construct and solve (14) to obtain $(\mathbf{u}^{*,m}_{n'}, \mathbf{v}^{*,m}_{n'})$ and $a^{*,m}_{n'}$, which denote the optimal solution and value for each sample, respectively. An estimate of $\mathbb{E}\{a^*_{n'}\}$, which is a lower bound for the true optimal value a^* can be estimated by $L_{n'}$, given by

$$L_{n'} = \frac{1}{M} \sum_{m=1}^{M} a^{*,m}_{n'}. \tag{15}$$

The upper bound, $\mathbb{E}\{f(\hat{\mathbf{u}}, \hat{\mathbf{v}})\}$ with a suboptimal solution $(\hat{\mathbf{u}}, \hat{\mathbf{v}})$, can be estimated using an evaluation sample of n'' iid observations $\{\xi^m_1, \xi^m_2, ..., \xi^m_{n''}\}$ simulated independently of the optimization set of n' scenarios. In particular, for $\mathbf{u}^{*,m}_{n'}, \mathbf{v}^{*,m}_{n'}$ at the m-th replication we have

$$U^m_{n''} = c(\mathbf{u}^{*,m}_{n'}, \mathbf{v}^{*,m}_{n'}) + \frac{1}{n''} \sum_{j=1}^{n''} Q(\mathbf{u}^{*,m}_{n'}, \mathbf{v}^{*,m}_{n'}, \xi^m_j). \tag{16}$$

It is preferred that the evaluation sample size be significantly higher than the optimization sample size, i.e., $n'' \gg n'$. For M replications, the upper bound estimate can be immediately computed as

$$U_{n''} = \frac{1}{M} \sum_{m=1}^{M} U^m_{n''}. \tag{17}$$

Let σ^2_L and σ^2_U be the standard sample variance of $L_{n'}$ and $U_{n''}$, respectively. We can compute a $(1-\alpha)$-confidence interval (CI) on the lower bound and the upper bound estimates as:

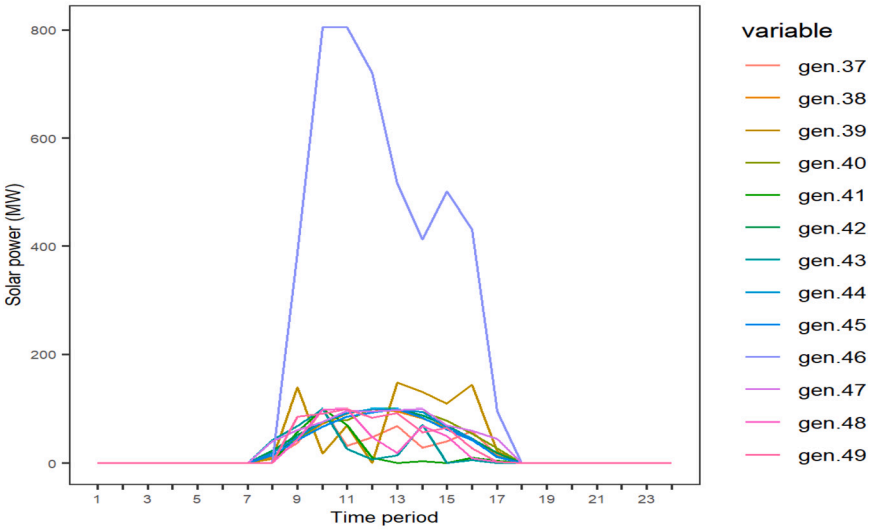

Fig. 3. Power at solar generators for the IEEE-118 system vs time.

$$\mathrm{CI}_L = \left[L_{n'} \pm \frac{\zeta_{a/2}\sigma_L}{\sqrt{M}}\right]; \quad \mathrm{CI}_U = \left[U_{n''} \pm \frac{\zeta_{a/2}\sigma_U}{\sqrt{M}}\right], \tag{18}$$

where $\zeta_{a/2}$ is the $(1-a/2)$ quantile of the standard normal distribution. We can define the worst-case optimality gap, which we refer to as the *pessimistic gap*, as the difference between the upper end of CI_U and the lower end of the CI_L. If the pessimistic gap is acceptably smaller than a threshold, then the SAA procedure is terminated with a statistical guarantee on the optimal objective value.

4. Numerical results

For our case study, we conduct experiments on two modified IEEE-57 and IEEE-118 bus systems. The data for these bus systems are available online in [44]. The IEEE-57 system has 7 generators of which 5 are conventional, and the remaining 2 are renewable (wind) generators. The IEEE-118 bus system has 54 generators of which 36 are conventional, and the remaining 18 are wind and solar generators. The scenarios of wind and solar generation are a simulated sample with size $n = 1000$. These scenarios were generated using a Vector Autoregressive (VAR) model whose parameters were estimated based on the historical data provided in [45]. The model parameter estimation and simulation were conducted on the *R* platform using `vars` and `MTS` packages. The LHS algorithm as well as fitting the MARS model is also performed in *R*. The optimization procedures for both the DACE approach and L-shaped method are conducted on a *C/C++* platform with CPLEX 12.9 as the solver on a Linux-based server running Ubuntu version 20.04.4 with a 3.60 GHz 8-Core Intel processor with 64 GB RAM.

In the original $\mathbf{x}$ space for the modified IEEE-57 bus system, there are 360 features for the 5 conventional generators, and the modified IEEE-118 bus system contains 2,592 features, which represent the 36 conventional generators over the 24-hour planning horizon. For the dimension of the $\mathbf{w}$ variables, we observe the patterns at the energy output of the simulated time series for different renewable generators that have a direct impact on whether conventional generators have to be operational or renewable units are adequate to meet the demand at that certain time period t. As illustrated in Fig. 3, solar power forecasts demonstrate a pattern of zero from time period $t = 1$ to $t = 7$. The peak of solar power is shown to be between $t = 8$ and $t = 17$, and finally from $t = 18$ to $t = 24$, we observe zero power once more. Based on these patterns, we set $\mathcal{I} = 3$ at different time lengths of $|\mathcal{T}_1| = 7$, $|\mathcal{T}_2| = 10$ and $|\mathcal{T}_3| = 7$ for each generator g. This results in 108 features in the $\mathbf{w}$ space for the modified IEEE-118 bus system and only 15 features for the IEEE-57 system. Specifically, the dimensionality reduction procedure allows the implementation of the LHS algorithm on 15 and 108 features instead of the original 360 and 2592 decision values for IEEE-57 and IEEE-118, respectively.

4.1. DoE procedure

In order to implement Algorithm 1, we consider $2 \times \Omega_g = 6$ as the overall number of remain-on and remain-off time periods for generator g. We have also set $\mathrm{MaxUT}_g = 24$ and $\mathrm{MaxDT}_g = 24$. As a rule of thumb, one might start with at least 2-3 times the number of features for the number of observations. For the commitment linking space, we initially consider $n = 300$ observations in the DoE process. Eliminating the observations that represented infeasible first-stage solutions in the IEEE-118 bus system due to constraints in (3) – (6) leaves us with 205 feasible design points. We noticed that out of the 108 predictors for this system, at most 20 of them were selected to appear in each MARS model. This means the required dimension was greatly reduced, and the 205 observations that were employed in our feasible experimental design were more than enough. The IEEE-57 bus system had no infeasible first-stage solutions, so all the design points were used. Once the sampled commitment decisions are obtained via the experimental design, we conduct the experiments in the following sections with $M = 30$ replicated scenarios of sample size $n' = 1000$.

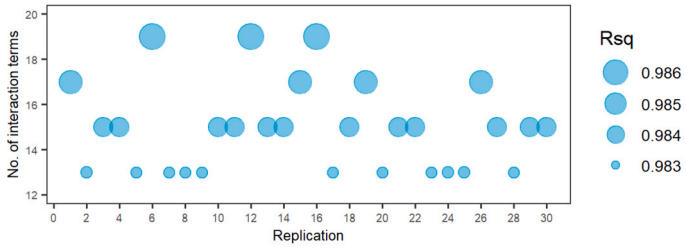

Fig. 4. Number of interaction terms for 30 replicated MARS models for the IEEE-118 system.

4.2. Optimization of the expected recourse function

The second-stage problem (7b) is solved using $n' = 1000$ generated random scenarios using the 300 design points for the IEEE-57 system and the 205 sampled design points as first-stage solutions for the IEEE-118 system. The expected recourse function is estimated to be the average of the second-stage recourse value over these scenarios.

4.3. MARS models

We use the `earth` package in *R*, Version 1.2.5033, to conduct the MARS algorithm in order to predict the expected recourse function. In our procedure, we observe that the replications merely differ in the interaction terms and not the main effects (i.e., the hinge functions are the same). Fig. 4 illustrates the number of interaction terms for the 30 replicated MARS models. While the average "R-squared" remains around 0.98 across the replications, the number of interaction terms varies between 13 and 19. The MARS procedure automatically chooses which variables are the most important ones to use, the positions of the knots in the hinge functions, and how the univariate hinge functions are combined.

4.3.1. Interpretability of MARS models

The constructed 30 MARS models help us interpret how the committed generators impact the operating costs as mentioned in the contribution. In particular, Fig. 5 captures the solution found using the first replicated MARS model at different time periods in the 24-hour horizon for IEEE-118. This figure shows that 11 of the conventional generators (out of 36) remain offline in the second part of the day ($\mathcal{T}_2$) in the presence of *renewable* energy. By contrast only 5 generators are offline in the first part of the day ($\mathcal{T}_1$), and no generator is offline in the third part of the day ($\mathcal{T}_3$). The presence of online generators in the first and third parts of the day is to compensate for the absence of renewable generation as seen previously in Fig. 3. For an example of the interaction terms at this replication and the plots of the one-way and two-way interactions, we refer the reader to Appendix D.

4.4. Optimization of the S-UCED model

Once we obtain the predicted recourse function, we can set $\hat{Q}$ as an approximation to the second stage problem (7b) and alternatively solve (13). Across $M = 30$ replications, we use the resulting optimal solutions as an input to solve the original S-UCED model using (14). This is our lower bound estimate, which we refer to it as the predicted value.

Since (14) has finite support, we can use the L-shaped method to solve the SAA problem. We use the results as a basis of comparison for our DACE-based approach. The SAA instance is solved using a sample size of $n' = 1000$ across the M replicated scenarios terminated at ϵ as the optimality gap. This gap is defined as the difference between the in-sample upper and lower bound within the acceptable tolerance of ϵ in the L-shaped optimization process. The results of solving the IEEE-57 and IEEE-118 instances with the two methods are summarized in Table 1. This table presents the predicted value, $L_{n'}$, for $n' = 1000$ which prescribes a solution for S-UCED, and the out-of-sample bound, $U_{n''}$, which we refer to as the validated value for $n'' = 10,000$, along with their standard deviations. We set $\epsilon = 5\%$ for the IEEE-57 instance. During the experiment, we noticed that the L-shaped method for this instance led to termination of all replications before it reached optimality, even with an imposed time limit of 12 hours for each replication; hence the results are reported with an average optimality gap of 17% for this example. The last column of Table 1 shows the average computational time. This time includes the overall time of executing each step of the two methods. Notice that the DACE approach reduces the overall computational time significantly compared to the L-shaped method for this example. We have also reported the pessimistic gap percentage in Table 1. As observed in the table, DACE does not necessarily offer a cheaper solution which is evident in the IEEE-57 results. However, DACE yields more consistent solutions in both instances compared to the L-shaped method as the lower standard deviations and lower pessimistic gap suggests. In other words, although the quality of the average solution measured by the validated value seems better in L-shaped for the IEEE-57 instance, the pessimistic gap percentage suggests that there is a much larger difference between what the optimization process in the L-shaped method predicted for the objective value and what was validated. For the IEEE-118 instance we noticed that within 5% of optimality, the DACE approach not only presents a lower predicted value than the optimal predicted value using the L-shaped method, the validated value for the DACE approach is on average 2% better than the L-shaped method, which is nearly 2 standard deviations. The pessimistic gap percentage for IEEE-118 is also significantly larger than the DACE approach. In this case, in order to allow the L-shaped method to find solutions that were

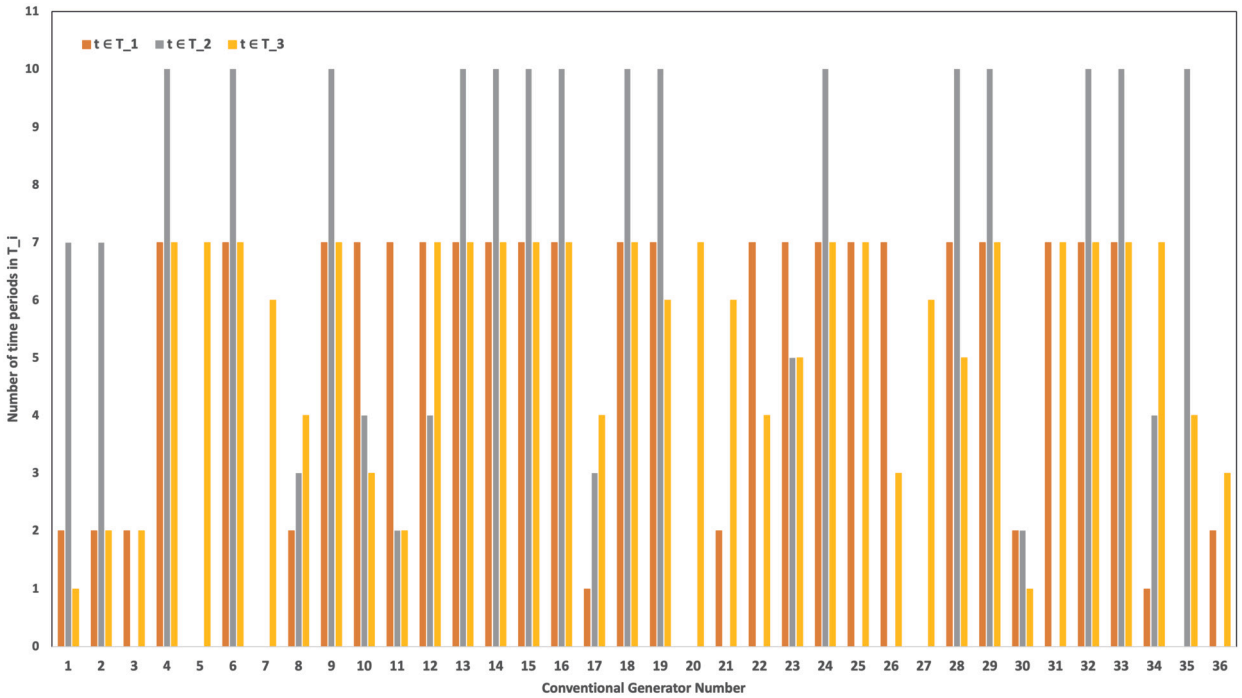

Fig. 5. Operational status of the conventional generators for replication 1 in the three time parts of the day (IEEE-118 bus system).

Table 1
Results from DACE vs. L-shaped for IEEE-57 and IEEE-118.

Algorithm	Predicted value ($L_{n'}$) (std. dev.)	Validated value ($U_{n''}$) (std. dev.)	Pessimistic gap (%)	Avg. time (H:M:S) (std. dev.)
IEEE-57				
DACE	$ 1,366,288.073 (1263.72)	$ 1,366,086.32 (1169.22)	0.05	01:22:04.86 (00:02:08.99)
L-shaped ($\epsilon = 5\%$)	$ 1,251,309.07 (12995.34)	$ 1,357,886.94 (77086.66)	10.22	12:00:34.02 (00:00:10.67)
IEEE-118				
DACE	$ 20,342,422.56 (3758.87)	$ 20,313,343.16 (3,184.38)	0.12	03:48:42.43 (00:00:55.75)
L-shaped ($\epsilon = 5\%$)	$ 20,405,894.14 (46023.65)	$ 20,705,285.06 (209,893.44)	1.89	01:23:33.17 (01:06:02.14)
L-shaped ($\epsilon = 1\%$)	$ 20,358,113.92 (34,892.90)	$ 20,630,973.13 (209,050.50)	1.75	07:29:39.26 (04:24:58.67)

more competitive with those of the DACE approach, we additionally solved the problem using L-shaped with $\epsilon = 1\%$. Despite setting a substantially lower optimality gap, the L-shaped method failed to outperform the solutions of DACE. This resulted in significantly longer computational times for each replication where half of them timed out after 12 hours, and the best average gap of 1.03% across all the replications was reported. As mentioned, the solutions obtained from the DACE approach show closer predicted and validated values as well as lower variability compared to the L-shaped solutions for both examples. This can be attributed to the fact that the replicated MARS models have low sensitivity toward the 30 replicated scenario sets as demonstrated in Fig. 4.

Next, we report the detailed average time results for each step of the DACE and L-shaped procedures in Table 2 and Table 3. Note that in both test systems, for the L-shaped method, solving the subproblems accounts for a considerable portion of the computational time. Since in the DACE approach, the commitment decisions in the first stage are generated using the proposed experimental design, the computational time to solve the recourse function is highly consistent with very little standard deviation, and in the cases of the IEEE-57 instance and the IEEE-118 instance with $\epsilon = 1\%$, considerably shorter on average compared to the L-shaped method (refer to Step 2 of average time for the DACE approach and the L-shaped method).

As depicted in Fig. 6, the mean differences of the IEEE-118 system's out-of-sample estimate (validated value) for the L-shaped method ($\epsilon = 1\%$) show a large variability across the 30 replicated values. This figure further demonstrates the consistent performance of the solutions using DACE.

5. Concluding remarks and future work

In this paper, we presented the first application of a DACE-based statistical approach to optimize the S-UCED with uncertainties in renewable generation. We proposed a creative, experimental design sampling specifically developed to simulate the first-stage decisions and solve the second-stage continuous recourse values. We presented a MARS approximation to predict the second-stage

Table 2
Computational Time for the DACE and L-shaped procedures (IEEE-57).

Step	Description	Avg time (H:M:S) (std. dev.)
DACE		
1	Generate LHS using Algorithm 1	00:00:15.20 (00:00:0.00)
2	Generate recourse function values	01:21:44.94 (00:02:08.81)
3	Fit a MARS approximation	00:00:04.62 (00:00:0.93)
4	Optimization to obtain the first stage solution	00:00:00.10 (00:00:0.04)
L-shaped ($\epsilon = 5\%$)		
1	Optimization of the Subproblems	08:03:09.69 (00:32:52.33)
2	Optimization of the Master problem	03:46:37.22 (00:33:34.71)

Table 3
Computational Time for the DACE and L-shaped procedures (IEEE-118).

Step	Description	Avg time (H:M:S) (std. dev.)
DACE		
1	Generate LHS using Algorithm 1	00:00:22.21 (0:0:0.00)
2	Generate recourse function values	03:48:19.40 (00:00:55.74)
3	Fit a MARS approximation	00:00:0.77 (00:00:0.02)
4	Optimization to obtain the first stage solution	00:00:0.48 (00:00:0.08)
L-shaped ($\epsilon = 5\%$)		
1	Optimization of the Subproblems	01:19:19.26 (01:02:03.01)
2	Optimization of the Master problem	00:03:22.87 (00:03:22.77)
L-shaped ($\epsilon = 1\%$)		
1	Optimization of the Subproblems	06:50:27.46 (03:57:55.06)
2	Optimization of the Master problem	00:34:38.78 (00:24:55.65)

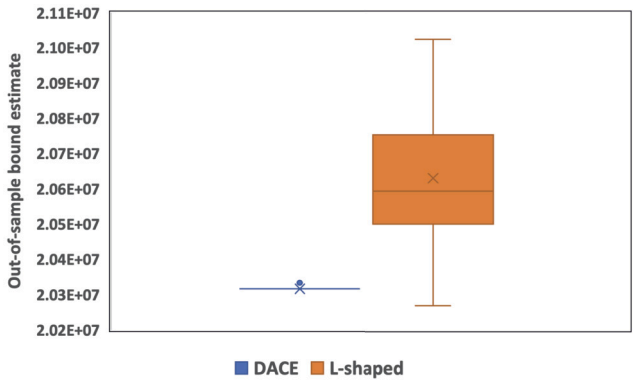

Fig. 6. Mean differences of out-of-sample estimate for DACE vs L-shaped (IEEE-118).

recourse function. This approach demonstrates great efficiency in approximating complex functions within optimization. In particular, the computational results on a large-scale test system (IEEE-118) and a medium-sized test system (IEEE-57) verify the significant computational improvement over the conventional L-shaped method where we use a multiple replication procedure to assess the quality of our stochastic solutions obtained from both methods. In addition, as a result of the significant reduction in the computational time of optimizing the SP model, this approach can be used as an alternative method to solve SP problems arising in power systems planning and operations applications within the common dedicated time frame considered in the electricity market. Future work will address additional approaches to tackle the challenge of generating DoE points that violate the valid inequalities in the UC model. Nonetheless, the design of experiments developed in this research can be used for a general system of devices or machines that either turn on or off with fixed lower and upper bounds on the on and off period. Consequently, another topic of future research is to apply the design of experiments approach to other applications with similar system characters, such as pre-timed control traffic signal timing with fixed cycle length [46]. In addition, the second stage ED model is known to be convex, so the efficient optimization of the MARS approximation with enforced convexity and using derivatives of the MARS function to generate cuts is also topics of future research.

Utilizing SAA in the optimization process necessitates the selection of the samples *a priori*. Since one subproblem is solved for each scenario, their relative performance is often problem-dependent. This often results in an increase in the computational time by

increasing the sample size. Sequential sampling algorithms such as the SD method [47] have been prevalent in tackling this issue. SD uses a sequence of approximations built by introducing new scenarios in every iteration. However, the SD method cannot handle discrete variables in the first stage. The development of a customized SD method is a subject for future work. Other approaches such as a decomposition method across scenarios in addition to the time periods can provide more information about the status of the generator when solving problems with varying scenarios. In our future research, we will investigate improvements to address these challenges in solving S-UCED models.

Declaration of competing interest

The authors declare that they have no known competing financial interests or personal relationships that could have appeared to influence the work reported in this paper.

Acknowledgements

Victoria Chen and Jay Rosenberger are currently supported by the National Science Foundation Award ECCS-1938895.

Appendix A. Nomenclature

Sets	
$\mathcal{T}$	Time scale decision epochs
$\mathcal{B}$	Buses
L	Transmission lines
$\mathcal{D}$	Demand
$\mathcal{G}$	Conventional generators
$\mathcal{R}$	Renewable generators
Generator Parameters	
$\underline{C}_g/\overline{C}_g$	Minimum/maximum required generation when g is operational
$\overline{R}_g/\underline{R}_g$	Ramp-up/ ramp-down limit at generator g
$\overline{S}_g/\underline{S}_g$	Start-up/ shut down limit at generator g
UT_g/DT_g	Minimum uptime/ downtime limit at generator g
$f^{SU}_{g,t}/f^{SD}_{g,t}$	Incurred startup/shutdown cost for generator g at time t
c^0_g	No-load cost at generator g
c^κ_g	Variable cost of the κth piece for generator g
d^{gs}_g	Shedding penalty at generator g
γ^κ_g	Production amount of the κth piece at generator g, $\kappa = \{1, .., \kappa^{max}\}$
$\hat{V}(\gamma^\kappa_g)$	Aggregated cost of generating γ^κ_g units of output
Bus and Line Parameters	
V	Bus voltage
$\theta^{min}, \theta^{max}$	Angle limits of the connected buses
p^{min}, p^{max}	Line capacity limits
X	Line reactance
Other Parameters	
$D_{i,t}$	Demand at demand node i at time t
ρ_t	The required reserve amount at time t
d^{ls}_i	Value of lost load at demand node i
$\tilde{G}_{g,t}$	Total amount of available renewable energy at the renewable generator g at time t
UC Decision Variables	
$x_{g,t}$	1 if g remains operational at period t, 0 otherwise
$s_{g,t}/\hat{z}_{g,t}$	1 if g is turned on/off, 0 otherwise
$G'_{g,t}$	Day-ahead production amount beyond $\underline{C}_g$ provided by generator g at time t
$\overline{G}_{g,t}$	Maximum day-ahead generation amount that g can supply at time t
ED Decision Variables	
$G_{g,t}$	Hour-ahead generation level at generator g at time t
$p_{(i,j),t}$	Power flow on line (i, j) at time t
r^{ls}_{it}	Load curtailment at demand node i
r^{gs}_{gt}	Generation curtailment at generator g at time t
θ_{it}	Angle of the node i at time t
$v_{g,t}$	Day-ahead generation cost amount of generator g at time t

Appendix B. Economic dispatch problem formulation

In the ED model, the system responds to a realized demand and renewable generation outcome by adapting actual generation levels of all generators committed in the UC solution. While the UC model ensures that the generation and demand quantities are balanced at a system-level, the ED problem incorporates a more detailed representation of the power network. For this purpose, we additionally define variables for power flow on a line $(i,j) \in L$, denoted $p_{(i,j),t}$, and phase angle $\theta_{i,t}$ for a node $i \in \mathcal{B}$ for all time periods $t \in \mathcal{T}$. In this stage, the generation resources are adjusted to the prevailing conditions, which may be different from the forecasts used in the day-ahead UC stage. The ED model that we present here is based on [17].

For generator g at each time period t, we assume that the hour-ahead generation cost $v_{g,t}$ is a piece-wise linear convex function of the dispatch amounts. Variables for the load curtailment at demand node i, r^{ls}_{it}, and generation curtailment at generator g, r^{gs}_{gt}, at time t are other components of the objective function given below.

$$\min \quad \sum_{t\in\mathcal{T}} \left(\sum_{g\in\mathcal{G}} v_{g,t} + \sum_{g\in\mathcal{G}\cup\mathcal{R}} d^{gs}_{g} r^{gs}_{g,t} + \sum_{i\in\mathcal{D}} d^{ls}_{i} r^{ls}_{i,t} \right). \tag{B.1}$$

Here, d^{gs}_{g} and d^{ls}_{i} are the shedding penalties for generator g and load at node i.

Since only committed generators are capable of generating within their capacities in the ED problem, they must satisfy the following constraints:

$$\underline{C}_g (x_{g,t} + s_{g,t}) \le G_{g,t} \le \overline{C}_g (x_{g,t} + s_{g,t}) \qquad \forall g \in \mathcal{G},\ t \in \mathcal{T}, \tag{B.2}$$

where $G_{g,t}$ is the hour-ahead generation level at generator g at time t. Similar to the UC model, ramping constraints are imposed on generation as follows:

$$G_{g,t} - G_{g,t-1} \le \overline{S}_g s_{g,t} + \overline{R}_g x_{g,t} \qquad \forall g \in \mathcal{G},\ t \in \mathcal{T}, \tag{B.3a}$$

$$G_{g,t-1} - G_{g,t} \le \underline{S} z_{g,t} + \underline{R}_g x_{g,t} \qquad \forall g \in \mathcal{G},\ t \in \mathcal{T}. \tag{B.3b}$$

Notice that the variable $G_{g,t}$ in ED is analogous to $G'_{g,t} + \underline{C}_g$ in the UC model, but $G_{g,t}$ and $G'_{g,t}$ are determined separately.

At each bus in the network, flow balance equations guarantee that the demand is satisfied through the available generation or through power flows on lines connected to the bus. The flow balance equations are presented below.

$$\sum_{j:(j,i)\in L} p_{ji,t} - \sum_{j:(i,j)\in L} p_{ij,t} + \sum_{j\in\mathcal{G}_i} \left(G_{j,t} - r^{gs}_{j,t} \right) + \sum_{j\in\mathcal{R}_i} \left(G_{j,t}(\tilde{\xi}) - r^{gs}_{j,t} \right) = \sum_{j\in\mathcal{D}_i} \left(D_{j,t} - r^{ls}_{j,t} \right) \quad \forall i \in \mathcal{B},\ t \in \mathcal{T}. \tag{B.4}$$

In the above, we use $\mathcal{G}_i \subseteq \mathcal{G}$ to denote the subset of generators that are connected to bus $i \in \mathcal{B}$. Similarly, $\mathcal{D}_i \subseteq \mathcal{D}$ and $\mathcal{R}_i \subseteq \mathcal{R}$ denote the subset of loads and renewable generators connected to bus i, respectively. In our model, we allow the excess generation (from both conventional and renewable resources) to be shed and demand to be curtailed. The amount of generation shed is captured by $r^{gs}_{g,t}$ and demand curtailment by $r^{ls}_{j,t}$.

The power flow on a transmission line $(i,j) \in L$ depends on the voltage set at the connected buses i and j. These quantities (power flows and voltages) are complex numbers that are connected through nonlinear relationships. In practice, a linear approximation that ignores the imaginary (reactive) part of power flow and line losses is commonly employed. We adopt such a linear or direct current (DC) approximation of the power flows. These are given by

$$p_{ij,t} = \frac{V_i V_j}{X_{ij}} (\theta_{i,t} - \theta_{j,t}) \quad \forall (i,j) \in L, t \in \mathcal{T}, \tag{B.5}$$

where parameter V_i is the voltage magnitude at bus i and parameter X_{ij} is the reactance of line (i,j).

The power flows, the voltage angles, the generation shedding, and load curtailment variables are bounded as follows:

$$p^{min}_{ij} \le p_{ij,t} \le p^{max}_{ij} \qquad \forall (i,j) \in L,\ t \in \mathcal{T}, \tag{B.6a}$$

$$\theta^{min}_{i} \le \theta_{i,t} \le \theta^{max}_{i} \qquad \forall i \in \mathcal{B}, t \in \mathcal{T}, \tag{B.6b}$$

$$0 \le r^{ls}_{i,t} \le D_{i,t} \qquad \forall i \in \mathcal{D},\ t \in \mathcal{T}, \tag{B.6c}$$

$$0 \le r^{gs}_{i,t} \le G_{i,t} \qquad \forall i \in \mathcal{G}\cup\mathcal{R},\ t \in \mathcal{T}, \tag{B.6d}$$

where θ^{min} and θ^{max} are the voltage angle limits, and p^{min} and p^{max} are line capacity limits.

The generation cost is a piecewise affine function of the generation amounts. If there are $\kappa^{\max}_g$ pieces for a generator $g \in \mathcal{G}$, then we denote the coefficient and the breakpoint by c^{κ}_g and γ^{κ}_g, respectively, for an individual piece $\kappa = 1, \ldots, \kappa^{\max}_g$. The coefficients satisfy $c^1_g \le c^2_g \le \ldots \le c^{\kappa^{\max}}_g$. The aggregate cost of generating $G_{g,t}$ units is represented by the function $\widehat{V}(G_{g,t})$. These costs are incorporated

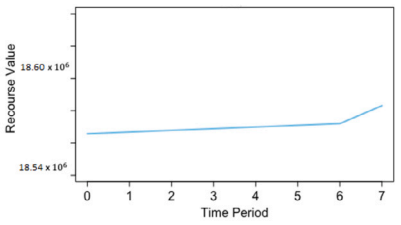

(a) Univariate hinge function for generator 7 at $\mathcal{T}_3$

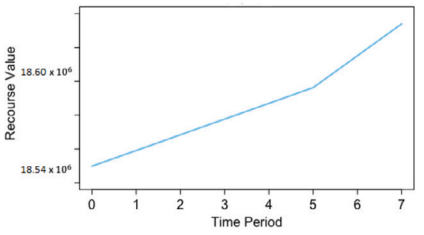

(b) Univariate hinge function for generator 25 at $\mathcal{T}_3$

Fig. D.7. The univariate terms of generators 7 and 25 in the third part of the day (IEEE-118).

in the model by using auxiliary variables $v_{g,t}$. With these definitions, we enforce the piecewise generation costs using the following constraints:

$$v_{g,t} \geq c_g^{\kappa}(G_{g,t} - \gamma_g^{\kappa-1}) + \widehat{V}_g(\gamma_g^{\kappa-1}) - \widehat{V}(\underline{C}_g) \quad \forall g \in \mathcal{G},\ t \in \mathcal{T}, \quad \kappa = 1, \ldots, \kappa^{max}. \tag{B.7}$$

The above ensures that the unit generation cost within interval $[\gamma_g^{\kappa}, \gamma_g^{\kappa+1}]$ is c_g^{κ}.

Appendix C. Decomposed multi-period two-stage S-UCED model

Using the UC and ED model components introduced in the previous sections, we next present the decomposed multi-period two-stage S-UCED models. In this model the UC problem constitutes the first stage, and the ED problem is the second stage. The two-stage S-UCED is given as

$$\min \quad \sum_{t\in\mathcal{T}} \left(\sum_{g\in\mathcal{G}} \left(f_{g,t}^{SU} s_{g,t} + f_{g,t}^{SD} z_{g,t} + \widehat{Q}(\underline{C}_g)(s_{g,t} + x_{g,t}) \right) \right) + \mathbb{E}\{h(x,s,z,\tilde{\xi})\} \tag{UC}$$

$$\text{s.t } (1)\text{-}(6),\ (x,s,z) \in \{0,1\}^{3|\mathcal{G}||\mathcal{T}|},\ (G', \overline{G}) \geq 0,$$

where,

$$h(x,s,z,\xi) = \min \quad \sum_{t\in\mathcal{T}} \left(\sum_{g\in\mathcal{G}} v_{g,t} + \sum_{g\in\mathcal{G}\cup\mathcal{R}} d_g^{gs} r_{g,t}^{gs} + \sum_{i\in\mathcal{D}} d_i^{ls} r_{i,t}^{ls} \right) \tag{ED}$$

$$\text{s.t } (B.2) - (B.7).$$

Appendix D. MARS interaction terms

Let us consider generator 25 from the IEEE-118 test system as an example. For this particular generator, the interaction terms of the first replicated MARS model have the following form:

$$1167.52 * \max(0, 6 - w_{7,2}) * \max(0, 5 - w_{25,3}) +$$

$$1464.66 * \max(0, w_{7,2} - 6) * \max(0, 5 - w_{25,3})$$

Moreover, Fig. D.7 depicts the univariate terms for variables $w_{7,3}$ and $w_{25,3}$ with knots at $k = 6$ and $k = 5$, respectively. Since the objective of the second stage is to minimize the ED problem, the recourse function would be minimized with generators 7 and 25 remaining offline in the third part of the day as shown in the univariate terms in Fig. D.7. However, in order to fulfill the demand in the second part of day, generator 7 should remain online since the costs decrease as its number of remaining online time periods increases. This is indicated in the first interaction term. However, due to its minimum uptime as well as the shedding penalty restrictions, this generator cannot remain online for more than 6 consecutive time periods. While having generator 25 online for more than 5 hours will reduce the interaction terms, it will increase the expected cost of shedding in the third part of the day due to the large coefficients of the univariate terms. Each graph in Fig. D.8 shows the interaction terms in the MARS model between two predictor variables at different periods of the day. For example, we observe the predicted value of Q, as $w_{27,2}$ and $w_{27,3}$ vary, with other variables fixed at their median values.

References

[1] B. Perciasepe, The clean energy transition is powering the U.S. economy, https://www.c2es.org/2017/04/the-clean-energy-transition-is-powering-the-u-s-economy. (Accessed 1 November 2020), 2017.

[2] Center for Climate and Energy Solutions, Renewable energy, https://www.c2es.org/content/renewable-energy/. (Accessed 15 November 2020), 2018.

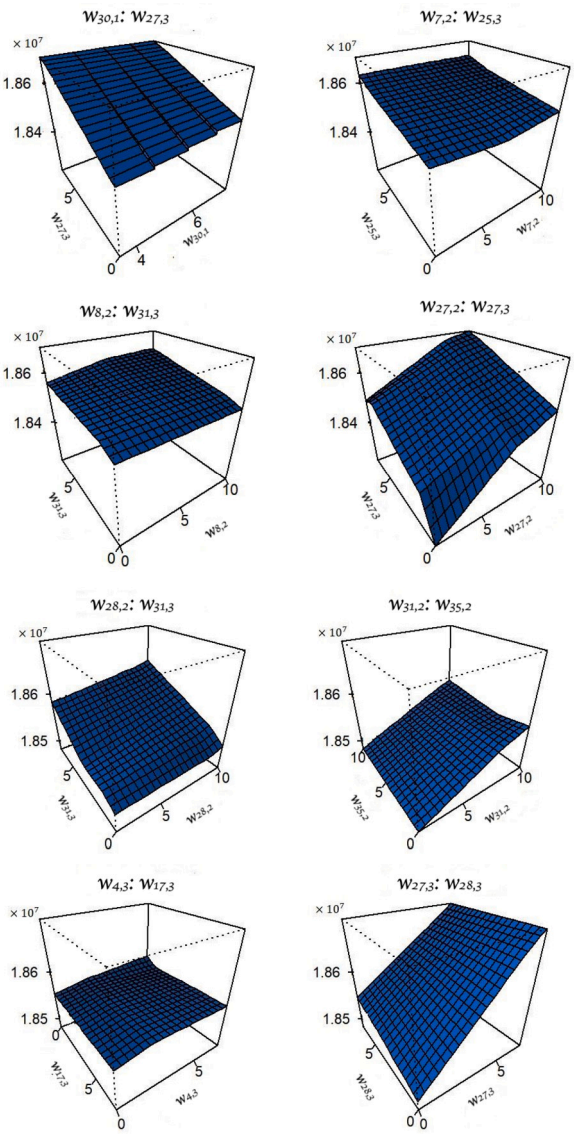

Fig. D.8. Interaction terms in the MARS model for IEEE-118.

[3] A. Fallahi, J.M. Rosenberger, V.C.P. Chen, W.-J. Lee, S. Wang, Linear programming for multi-agent demand response, IEEE Access 7 (2019) 181479–181490, https://doi.org/10.1109/ACCESS.2019.2959727.

[4] S. Atakan, H. Gangammanavar, S. Sen, Towards a sustainable power grid: stochastic hierarchical planning for high renewable integration, Eur. J. Oper. Res. 302 (1) (2022) 381–391, https://doi.org/10.1016/j.ejor.2021.12.042.

[5] G. Osório, J. Lujano-Rojas, J. Matias, J. Catalão, A probabilistic approach to solve the economic dispatch problem with intermittent renewable energy sources, Energy 82 (2015) 949–959, https://doi.org/10.1016/j.energy.2015.01.104.

[6] R. Wiebking, Stochastische modelle zur optimalen Lastverteilung in einem Kraftwerksverbund, ZOR, Z. Oper.-Res. 21 (6) (1977) B197–B217, https://doi.org/10.1007/BF01918361.

[7] S. Takriti, J. Birge, E. Long, A stochastic model for the unit commitment problem, IEEE Trans. Power Syst. 11 (3) (1996) 1497–1508, https://doi.org/10.1109/59.535691.

[8] R.T. Rockafellar, R.J.-B. Wets, Scenarios and policy aggregation in optimization under uncertainty, Math. Oper. Res. 16 (1) (1991) 119–147.

[9] P. Carpentier, G. Gohen, J.-C. Culioli, A. Renaud, Stochastic optimization of unit commitment: a new decomposition framework, IEEE Trans. Power Syst. 11 (2) (1996) 1067–1073, https://doi.org/10.1109/59.496196.

[10] T. Shiina, J.R. Birge, Stochastic unit commitment problem, Int. Trans. Oper. Res. 11 (1) (2004) 19–32, https://doi.org/10.1111/j.1475-3995.2004.00437.x.

[11] J. Wang, M. Shahidehpour, Z. Li, Security-constrained unit commitment with volatile wind power generation, IEEE Trans. Power Syst. 23 (3) (2008) 1319–1327, https://doi.org/10.1109/TPWRS.2008.926719.

[12] D. Bertsimas, E. Litvinov, X.A. Sun, J. Zhao, T. Zheng, Adaptive robust optimization for the security constrained unit commitment problem, IEEE Trans. Power Syst. 28 (1) (2012) 52–63, https://doi.org/10.1109/TPWRS.2012.2205021.

[13] Q.P. Zheng, J. Wang, A.L. Liu, Stochastic optimization for unit commitment—a review, IEEE Trans. Power Syst. 30 (4) (2014) 1913–1924, https://doi.org/10.1109/TPWRS.2014.2355204.

[14] W. Ackooij, I. Danti, F. Antonio, F. Lacalandra, M. Tahanan, Large-scale unit commitment under uncertainty: an updated literature survey, Ann. Oper. Res. 271 (2018) 11–85, https://doi.org/10.1007/s10479-018-3003-z.
[15] K. Liu, J. Zhong, Generation dispatch considering wind energy and system reliability, in: IEEE PES General Meeting, IEEE, 2010, pp. 1–7.
[16] J. Hetzer, C.Y. David, K. Bhattarai, An economic dispatch model incorporating wind power, IEEE Trans. Energy Convers. 23 (2) (2008) 603–611, https://doi.org/10.1109/TEC.2007.914171.
[17] H. Gangammanavar, S. Sen, V.M. Zavala, Stochastic optimization of sub-hourly economic dispatch with wind energy, IEEE Trans. Power Syst. 31 (2) (2015) 949–959, https://doi.org/10.1109/TPWRS.2015.2410301.
[18] A. Papavasiliou, S. Oren, Multiarea stochastic unit commitment for high wind penetration in a transmission constrained network, Oper. Res. 61 (3) (2013) 578–592, https://doi.org/10.2307/23474004.
[19] N. Sakhavand, H. Gangammanavar, Subproblem sampling vs. scenario reduction: efficacy comparison for stochastic programs in power systems applications, Energy Syst. (2022), https://doi.org/10.1007/s12667-022-00558-9.
[20] R.M. Van Slyke, R. Wets, L-shaped linear programs with applications to optimal control and stochastic programming, SIAM J. Appl. Math. 17 (4) (1969) 638–663.
[21] A. Shapiro, D. Dentcheva, A. Ruszczynski, Lectures on Stochastic Programming: Modeling and Theory, second edition, Society for Industrial and Applied Mathematics, Philadelphia, PA, USA, 2014.
[22] Q. Wang, Y. Guan, J. Wang, A chance-constrained two-stage stochastic program for unit commitment with uncertain wind power output, IEEE Trans. Power Syst. 27 (1) (2011) 206–215, https://doi.org/10.1109/TPWRS.2011.2159522.
[23] Y. Liu, N.-K.C. Nair, A two-stage stochastic dynamic economic dispatch model considering wind uncertainty, IEEE Trans. Sustain. Energy 7 (2) (2015) 819–829, https://doi.org/10.1109/TSTE.2015.2498614.
[24] K. Cheung, D. Gade, C. Silva-Monroy, S.M. Ryan, J.-P. Watson, R.J.-B. Wets, D.L. Woodruff, Toward scalable stochastic unit commitment, Energy Syst. 6 (3) (2015) 417–438, https://doi.org/10.1007/s12667-015-0148-6.
[25] J. Sacks, W.J. Welch, T.J. Mitchell, H.P. Wynn, Design and analysis of computer experiments, Stat. Sci. 4 (4) (1989) 409–423, https://doi.org/10.1214/ss/1177012413.
[26] V.C. Chen, Measuring the goodness of orthogonal array discretizations for stochastic programming and stochastic dynamic programming, SIAM J. Optim. 12 (2) (2002) 322–344, https://doi.org/10.1137/S1052623498332403.
[27] V.L. Pilla, J.M. Rosenberger, V.C. Chen, N. Engsuwan, S. Siddappa, A multivariate adaptive regression splines cutting plane approach for solving a two-stage stochastic programming fleet assignment model, Eur. J. Oper. Res. 216 (1) (2012) 162–171, https://doi.org/10.1016/j.ejor.2011.07.008.
[28] V.C. Chen, D. Ruppert, C.A. Shoemaker, Applying experimental design and regression splines to high-dimensional continuous-state stochastic dynamic programming, Oper. Res. 47 (1) (1999) 38–53, https://doi.org/10.1287/opre.47.1.38.
[29] N. Martinez, H. Anahideh, J. Rosenberger, D. Martinez, V.C. Chen, B. Wang, Global optimization of non-convex piecewise linear regression splines, J. Glob. Optim. 68 (2017) 563–586, https://doi.org/10.1007/s10898-016-0494-5.
[30] X. Ju, J.M. Rosenberger, V.C. Chen, F. Liu, Global optimization on non-convex two-way interaction truncated linear multivariate adaptive regression splines using mixed integer quadratic programming, Inf. Sci. 597 (1) (2022) 38–52, https://doi.org/10.1016/j.ins.2022.03.041.
[31] D.K. Lin, T.W. Simpson, W. Chen, Sampling strategies for computer experiments: design and analysis, Int. J. Reliab. Appl. 2 (3) (2001) 209–240.
[32] H. Patterson, The errors of lattice sampling, J. R. Stat. Soc. B 16 (1) (1954) 140–149, https://doi.org/10.1111/j.2517-6161.1954.tb00156.x.
[33] M.D. McKay, R.J. Beckman, W.J. Conover, A comparison of three methods for selecting values of input variables in the analysis of output from a computer code, Technometrics 21 (2) (1979) 239–245, https://doi.org/10.1080/00401706.1979.10489755.
[34] V.C. Chen, K.-L. Tsui, R.R. Barton, M. Meckesheimer, A review on design, modeling and applications of computer experiments, IIE Trans. 38 (4) (2006) 273–291, https://doi.org/10.1080/07408170500232495.
[35] V.L. Pilla, J.M. Rosenberger, V.C. Chen, B. Smith, A statistical computer experiments approach to airline fleet assignment, IIE Trans. 40 (5) (2008) 524–537, https://doi.org/10.1080/07408170701759734.
[36] J.H. Friedman, Multivariate adaptive regression splines, Ann. Stat. 19 (1) (1991) 1–67, https://doi.org/10.1214/aos/1176347963.
[37] S. Atakan, G. Lulli, S. Sen, A state transition MIP formulation for the unit commitment problem, IEEE Trans. Power Syst. 33 (1) (2017) 736–748, https://doi.org/10.1214/aos/1176347963.
[38] R.L. Mason, R.F. Gunst, J.L. Hess, Statistical Design and Analysis of Experiments: with Applications to Engineering and Science, first edition, John Wiley & Sons, 1989.
[39] M. Kutner, C. Nachtsheim, J. Neter, Applied linear regression model, vol. 26, https://doi.org/10.2307/1269508, 2004.
[40] B. Ariyajunya, Y. Chen, V.C. Chen, S. Kim, J. Rosenberger, Addressing state space multicollinearity in solving an ozone pollution dynamic control problem, Eur. J. Oper. Res. 289 (2) (2021) 683–695, https://doi.org/10.1016/j.ejor.2020.07.014.
[41] Y. Chen, F. Liu, J.M. Rosenberger, V.C. Chen, A. Kulvanitchaiyanunt, Y. Zhou, Efficient approximate dynamic programming based on design and analysis of computer experiments for infinite-horizon optimization, Comput. Oper. Res. 124 (2020) 105032, https://doi.org/10.1016/j.cor.2020.105032.
[42] W.-K. Mak, D.P. Morton, R.K. Wood, Monte Carlo bounding techniques for determining solution quality in stochastic programs, Oper. Res. Lett. 24 (1–2) (1999) 47–56, https://doi.org/10.1016/S0167-6377(98)00054-6.
[43] A.J. Kleywegt, A. Shapiro, T. Homem-de Mello, The sample average approximation method for stochastic discrete optimization, SIAM J. Optim. 12 (2) (2002) 479–502, https://doi.org/10.1137/S1052623499363220.
[44] R.D. Christie, Power systems test case archive, Online: http://www.ee.washington.edu/research/pstca/, 08.1999. (Accessed 1 December 2018).
[45] USC3DLAB, Two-stage stochastic decomposition, https://github.com/USC3DLAB/SD.git. (Accessed 31 December 2020), 2019.
[46] Transportation Research Board and National Academies of Sciences Engineering and Medicine, Signal Timing Manual, second edition, The National Academies Press, 2015.
[47] J.L. Higle, S. Sen, Stochastic decomposition: an algorithm for two-stage linear programs with recourse, Math. Oper. Res. 16 (3) (1991) 650–669, https://doi.org/10.1287/moor.16.3.650.